Vol 18 No 10, October 2009
1674-1056/2009/18(10)/4564–07

Chinese Physics B

© 2009 Chin. Phys. Soc.
and IOP Publishing Ltd

Electrochemical properties of SnO_2 nanorods as anode materials in lithium-ion battery*

Shi Song-Lin(施松林)†, Liu Yong-Gang(刘永刚),
Zhang Jing-Yuan(张敬源), and Wang Tai-Hong(王太宏)

Institute of Physics, Chinese Academy of Sciences, Beijing 100190, *China*

(Received 9 March 2009; revised manuscript received 30 April 2009)

Well-dispersed SnO_2 nanorods with diameter of 4–15 nm and length of 100–200 nm are synthesised through a hydrothermal route and their potential as anode materials in lithium-ion batteries is investigated. The observed initial discharge capacity is as high as 1778 mA·h/g, much higher than the theoretical value of the bulk SnO_2 (1494 mA·h/g). During the following 15 cycles, the reversible capacity decreases from 929 to 576 mA·h/g with a fading rate of 3.5% per cycle. The fading mechanism is discussed. Serious capacity fading can be avoided by reducing the cycling voltages from 0.05–3.0 to 0.4–1.2 V. At the end, SnO_2 nanorods with much smaller size are synthesized and their performance as anode materials is studied. The size effect on the electrochemical properties is briefly discussed.

Keywords: SnO_2 nanorods, lithium-ion battery, anode materials, fading mechanism
PACC: 8640, 8230F, 6146

1. Introduction

Lithium-ion batteries are widely used in portable electronic devices, hybrid electric vehicles, clean energy storage and aerospace, etc.[1,2] Graphite is the presently popular anode material with a maximum theoretical specific capacity of 372 mA·h/g.[3] Further improvements are required to meet the demand of higher energy capacity in the above-mentioned areas nowadays.[4] A possible route is finding alternative anode materials with higher capacities. Recently, transition-metal oxide nanostructures as anode materials in lithium-ion battery have attracted much attention. In comparison to conventional graphite, these novel anode materials have larger surface-to-volume ratio, shorter diffusion length, enhanced surface electrochemical reactivity and higher capacity for Li ions.[5−10] Among the transition-metal oxides, SnO_2 has a theoretical charge-storage capacity of 781 mA·h/g when forming alloy $Li_{4.4}Sn$,[11] twice of that in graphite. Because of their high capacities and relatively low potential for Li ion intercalation, various SnO_2 nanostructures, such as nanoparticles, nanowires and hollow spheres have been investigated as anode materials in lithium-ion battery.[12−15] Here we report well-dispersed SnO_2 nanorods with very high surface-to-volume ratio as anode materials, which show an initial discharge capacity of 1778 mA·h/g, much higher than the theoretical value of the bulk SnO_2. Serious capacity fading is observed and the mechanism is analysed. Furthermore, the size effect of SnO_2 nanorods on the electrochemical properties is briefly discussed at the end of the paper.

2. Experimental methods

Massive SnO_2 nanorods were synthesized by a hydrothermal method with precursors of $SnCl_4{\cdot}5H_2O$ and NaOH.[16] In a typical process, 2 mL $SnCl_4{\cdot}5H_2O$ (0.5 mol/L) and 5 mL NaOH (5 mol/L) were thoroughly mixed in 33 mL water/ethanol solution. After stirring for ∼10 min, the mixture was transferred into a 50-mL Teflon-lined autoclave and kept at 200 °C for 24 h. The products were harvested by repeatedly rinsing in deionized water and certificating for three times. Mass production and nontoxic reagents make this synthesis method very attractive.

The general morphology and crystal structure of the products were characterised by scanning electron microscope (SEM; JEOL-JSM-6700F), transmission electron microscope (TEM; TECNAI F20) and x-ray

*Project supported by the National Key Basic Research Program of China (Grant No 2007CB310500) and the Chinese Ministry of Education (Grant No 705040), the National Natural Science Foundation of China (Grant Nos 90606009, 60571044 and 10774174).
†Corresponding author. E-mail: slshi82@gmail.com

powder diffraction (XRD; D/max 2550 V, Cu Kα radiation). The surface area of the products was measured by the physical absorption of N_2 molecules using the BET method.

The lithium-ion batteries for the following test were assembled in an argon filled glove box.[17] A suspension was prepared by mixing SnO_2 nanorods, carbon black and polyvinylidene fluoride (PVDF) with the mass ratio of 85:10:5. The slurry was then coated onto a copper foil substrate. The electrode sheet was dried at 120 °C for 12 h in vacuum condition. Li foil was used as counter electrode. The electrolyte was made of 1 M $LiPF_6$ dissolved in a mixture composed of ethylene carbonate (EC) and dimethyl carbonate (DMC) with the volume ratio of 1:1. The galvanostatic charge–discharge measurements were carried out on a Land® multichannel galvanostat/potentiostat instrument at room temperature (∼20 °C) with a current density of 0.2 mA/cm^2. The cycling voltages were 0.05–3.0 V and 0.4–1.2 V, respectively.

3. Results and discussion

Figures 1(a) and 1(b) are typical SEM images of the SnO_2 nanorods synthesised at 200 °C for 24 h. The diameter and length of the nanorods are 4–15 nm and 100–200 nm, respectively. Each of the nanorods has one end outside with another end bound to other nanorods, exhibiting peculiar flower-like structures. When they form into a film, the surface area of the nanorods can be effectively used. Furthermore, due to the small diameter character of the nanorods, the diffusion length for Li ions is very short. These advantages facilitate the as-synthesised SnO_2 nanorods as anode materials in lithium-ion battery.

The TEM image of a typical SnO_2 nanorod is shown in Fig.1(c). The single nanorod is a single crystalline and has very clean surfaces. The spacing between two adjacent lattice planes is 0.332 nm, corresponding to (110) planes of tetragonal rutile SnO_2. The XRD pattern of the as-synthesised nanorods is shown in Fig.1(d). All the diffraction peaks agree with the reported values ($a = 0.474$ nm and $c = 0.318$ nm)

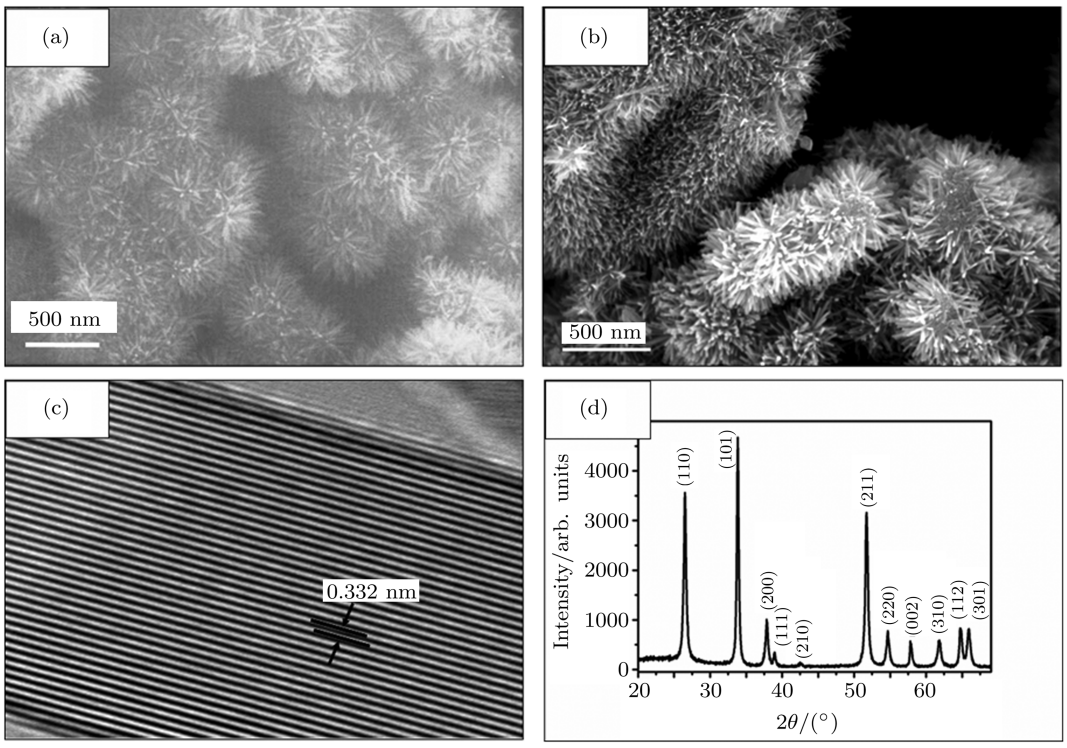


Fig.1. (a) and (b) typical SEM images of the SnO_2 nanorods synthesized at 200°C. The diameter and length of the nanorods are 4–15 nm and 100–200 nm, respectively. (c) TEM image of a typical SnO_2 nanorod. (d) XRD pattern indicating that the SnO_2 nanorods have crystal structure of rutile with calculated lattice parameters $a = 0.474$ nm and $c = 0.318$ nm.

from JCPDS card (41–1445) or the results in the literature,[16] confirming that the products are SnO_2 nanorods with rutile crystal structure. No peaks of impurities are seen in the XRD pattern, suggesting the high purity of the nanorods. Additionally, the peaks are relatively broadened compared to those of the bulk SnO_2, further indicating the small size of the nanorods.

The first discharge (Li insertion) and charge (Li extraction) voltage profiles of the cell are shown in Fig.2(a). In the first discharging process, the potential drops rapidly to a plateau of ∼1.0 V and then decreases gradually to ∼0.05 V. The plateau around 1.0 V corresponds to the formation of Li_2O and Sn,[11] which only exists during the first discharge process and almost disappears in the following cycles as shown in Fig.2(b). This process, as expressed by $SnO_2 + 4Li^+ + 4e^- \rightarrow Sn + 2Li_2O$, is unavoidable and irreversible. The stored Li cannot be released which are corresponding to the capacity loss of the first cycle.

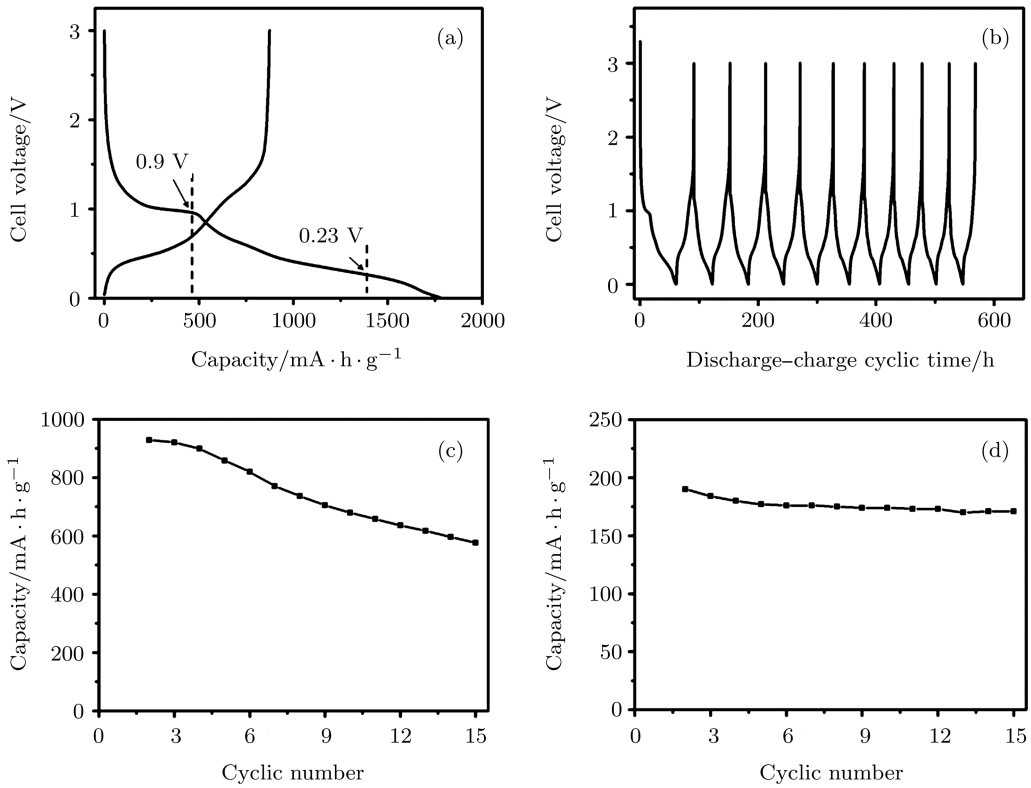


Fig.2. For the SnO_2 nanorods synthesised at 200 °C: (a) The curves in the first discharge–charge process. The initial discharge capacity is as high as 1778 mA·h/g. (b) Cycling of electrochemical Li insertion and extraction in SnO_2 nanorods. (c) Cycling electrochemical performance at the cell voltage of 0.05–3.0 V. (d) Cycling electrochemical performance at the cell voltage of 0.4–1.2 V.

As the insertion of lithium ions goes on, the cell voltage falls below 0.9 V. Li_xSn alloys will form from $Sn + xLi^+ + xe^- \leftrightarrow Li_x\,Sn$ $(0 \le x \le 4.4)$, which are Li_2Sn_5, LiSn, Li_7Sn_3, $Li_{13}Sn_5$, Li_7Sn_2 and $Li_{22}Sn_5$ in order. This reaction is reversible and Li can be released from the Li_xSn alloy when it decomposes in the charge process. During the first discharging process, the single-crystalline SnO_2 nanorods change to polycrystalline by intercalation of Li ions. Lithia matrix forms during the initial stage of Li insertion and holds the Li_xSn alloy regions together through the large volume changes in the alloying and dealloying processes.[18] The cycling performance of electrochemical Li insertion and extraction in SnO_2 nanorods is shown in Fig.2(b). We can see that the SnO_2 nanorods working in the low-potential range (0.05–1.6 V vs. Li/Li^+) is of use as active negative electrode materials in lithium-ion battery.

The lithium ions stored by the carbon black are neglectable as its mass and capability are much less than those of SnO_2 nanorods. The observed first (1778 mA·h/g) and second specific discharge capacities (929 mA·h/g) of SnO_2 nanorods are also much larger than the theoretical capacities of the bulk SnO_2 (1494 mA·h/g for the first discharge and 781 mA·h/g for the second).[11] The improved capacity is mainly due to the abundant surface defects, as well as the characters of high surface-to-volume ratio and good dispersity of the SnO_2 nanorods, which would effectively enhance the surface electrochemical reactivity and improve Li ion storage capacity. The extra Li-storage capacity in nanometer-sized transition-metal oxides has recently been explained by an interfacial Li storage mechanism.[19,20] According to this model, Li ions are stored on the ionic conducting side of the interface Li_2O. The Li_2O surface layers or the interfacial core serve as hosts for Li ions. Electrons are localised on the metallic side as it serves as an electron sink, resulting in a charge separation. It is consistent with the initial discharge profile. As shown in Fig.2(a), the Li_xSn alloys form during the cell voltage 0.9 V to 0.23 V. The $Li_{22}Sn_5$ alloys exhibit no further change as the voltage falls below 0.23 V.[11] However, the Li storage goes on and about 310 mA·h/g of the total 1778 mA·h/g occurs in the range of 0.23–0.05 V. Carbon black can store some Li ions as the voltage is lower than 0.23 V. However, it cannot be the key reason, for the mass ratio of SnO_2 nanorods and carbon black is 8.5:1 and the capacity of carbon is much smaller. The occurrence of an extra Li storage at low voltage is most probably caused by interfacial charge storage. Electrons are localized on $Li_{22}Sn_5$ side and Li ions on the Li_2O surface layers or the interfacial core.

The galvanostatic cycling profiles of the SnO_2 nanorods are shown in Fig.2(c). The reversible capacity decreases from 929 to 576 mA·h/g with a capacity fading of 3.5% per cycle during the successive 15 cycles. The increasing irreversible capacity is mainly due to the induced volume expansion. Serious volume expansion of the nanorods accompanies the Li insertion process and the schematic process is shown in Fig.3. Compared to pure Sn, the calculated volume increase factors for LiSn, Li_7Sn_3, Li_5Sn_2, $Li_{13}Sn_5$, Li_7Sn_2 and $Li_{22}Sn_5$ are 1.53, 2.28, 2.76, 2.81, 2.99 and 3.59, respectively.[11] When the anodes work at the voltage ranging from 0.05 V to 3.0 V, serious volume expansion happens in realising the $Li_{22}Sn_5$ phase and may cause two results. One is the cracking and crumbling of the anode materials. The anodes endure the strain of expansion of $Li_{22}Sn_5$. Therefore, the anode materials may crack, reducing the capacity. The other result is the aggregation of Sn crystallites into large regions. As the volume expanses seriously, the neighbouring Li_xSn alloys will join together. This process goes on with the cycling and the $Li_{22}Sn_5$ grows bigger. As a result, the Li atoms inside cannot be extracted out, causing the capacity fading. Additionally, the anodes operating at voltages 0.05–3.0 V are outside the electrochemical stability window (1.2 V) of the electrolyte components, the electrolyte will decompose and form SEI films. It has been found that the thick SEI films may disappear completely when catalyzed by transition metal upon Li extraction, which may lead to capacity fading.

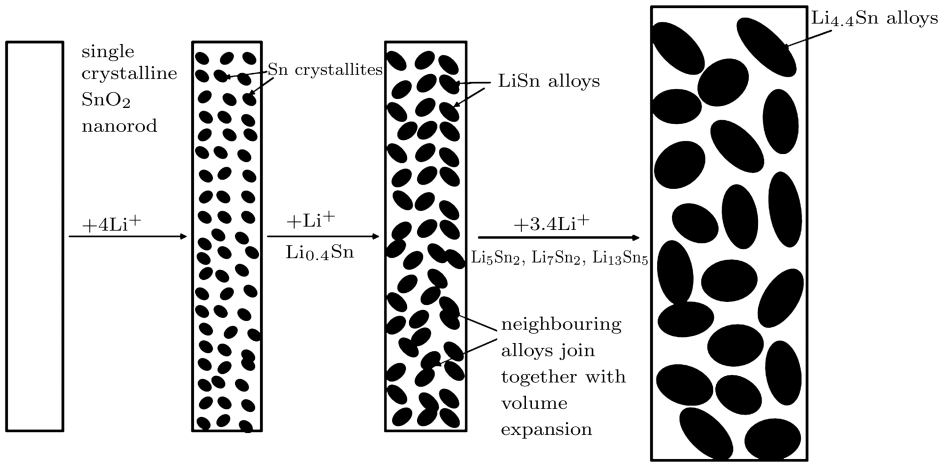


Fig.3. Schematic process of Li insertion accompanied with serious volume expansion.

If higher potential regions are avoided, the SnO_2 nanorods should show better cyclic ability according to the fading mechanism mentioned above. The performance of the cells cycled between 0.4 V and 1.2 V is shown in Fig.2(d). Although the second discharge capacity decreases to 190 mA·h/g, the capacity retention is improved. Even after 15 cycles, 92% of the capacity remains. The reduction of the cycling voltage improves the capacity fading through the following two ways and the results are consistent with the fading mechanism. (i) Reduce the volume expansion. The SnO_2 nanorods cycled between 0.4–1.2 V may only form LiSn phase and can avoid the presence of lower Li–Sn alloy phases (Li_7Sn_3, Li_5Sn_2, $Li_{13}Sn_5$, Li_7Sn_2 and $Li_{22}Sn_5$). So by adjusting the voltage limits to 0.4–1.2 V, serious volume expansion can be avoided. (ii) Reduce the SEI films decomposition. By limiting the cycling voltage from 0.05–3.0 V to 0.4–1.2 V, thinner SEI films will form and they become more stable, thus reducing the capacity fading. Besides the reduction of the cycling voltage, it has been reported that carbon coating and glass-forming elements adding can also be used to reduce the capacity fading. The carbon coating layers can significantly enhance the electronic conductivity of electrode materials and lead to stabilized SEI films, resulting in improved rate and cycling performance.[21] Glass-forming elements, such as B, P, and Al, can form stable framework and delocalises the Sn active center, avoiding the aggregation of Sn crystallites.[22]

SnO_2 nanorods with smaller size were synthesised by reducing the reaction temperature to 160 °C and their performance as anode materials was also investigated. A typical SEM image of the products is shown in Fig.4(a) with a TEM image shown in the top-right inset. The diameter and length of the nanorods are 3–9 nm and 20–40 nm, respectively; both are smaller than the nanorods synthesised at 200 °C. Figure 4(b) indicates that the initial discharge and charge capacities are 1519 and 647 mA·h/g, respectively. As shown in Fig.4(c), the reversible capacity decreases from 753 to 430 mA·h/g with a capacity fading of 4.5% per cycle. In comparison to the nanorods synthesised at 200 °C, the total and reversible capacities are much lower, and the capacity fading is faster.

The nanorods with smaller diameter should have better performance, because they have much higher surface-to-volume ratio and the surface electrochemical reactivity of a material is directly related to it. Different researchers have pointed out that the reversible

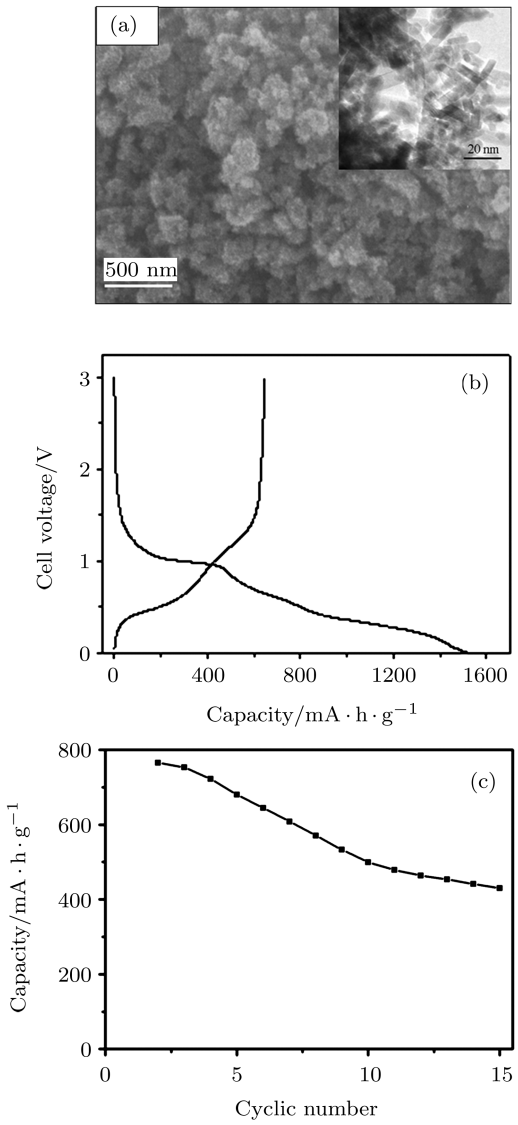


Fig.4. (a) A typical SEM image of SnO_2 nanorods synthesised at 160 °C. The inset is a TEM image of the as-synthesised nanorods. The diameter and length are 3–9 nm and 20–40 nm, respectively. (b) The first discharge-charge curves of SnO_2 nanorods synthesised at 160 °C. The initial discharge and charge capacities are 1519 and 647 mA·h/g. (c) Cycling electrochemical performance at the cell voltage of 0.05–3.0 V of SnO_2 nanorods synthesised at 160 °C.

capacity increases drastically with decreasing particle size,[11,23–26] while the SnO_2 nanorods show opposite behaviors in our results. To compare the electrochemical performances, cyclic voltammograms of SnO_2 nanorods synthesised at 160 °C and 200 °C during the second cycle are presented in Fig.5. The peak positions have no obvious difference. The peak separation is a little larger for SnO_2 nanorods synthesised at 200 °C. The weak reduction peak around 0.89 V derives from Li_2O formation as expressed by $SnO_2 + 4Li^+ + 4e^- \rightarrow Sn + 2Li_2O$, which mainly occurs in

the initial cycle. However, the irreversible reaction still takes place in the second cycle, suggesting the Li ions insertion into the interior of the materials. The pair of reduction and oxidation peaks at 0.15 V and 0.55 V is related to the decomposition and formation of Li_xSn.

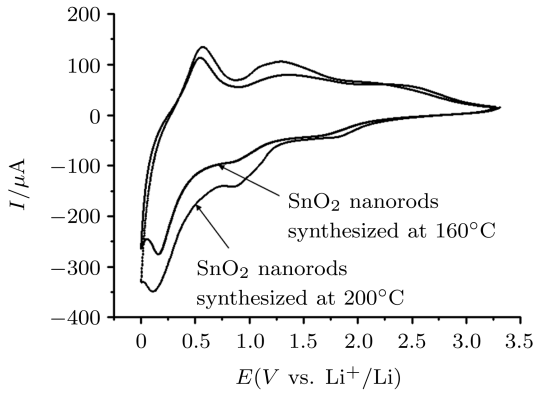


Fig.5. Cyclic voltammograms of SnO_2 nanorods synthesized at 160 °C and 200 °C during the second cycle at a scan rate of 0.1 mV/s.

As shown in Fig.5, the peak current I_p and the reversible capacities are much smaller for SnO_2 nanorods synthesised at 160 °C. It is mainly ascribed to the decrease of the effective surface area in the film composed of SnO_2 nanorods with smaller diameter. As shown in Figs.1(a) and 1(b), the nanorods synthesised at 200 °C exhibit flower-like structures which facilitate forming a loose film with large effective surface area and thus facilitate the insertion of Li ions. However, for the film composed of the nanorods synthesised at 160 °C, the specific surface area will get smaller due to serious aggregation. The aggregation makes the contact between SnO_2 nanorods and carbon black worse and reduces the utilisation of anode materials. As known, the peak current I_p is related to the reactant concentration n and can be expressed as $I_p \propto n^{3/2}$. The larger surface area of SnO_2 nanorods means a larger portion of the anode materials that contribute to Li ions storage, corresponding to a bigger reactant concentration. Thus the SnO_2 nanorods synthesised at 200 °C show higher peak current and Li ions storage capacity.

The specific surface areas of the nanorods were measured using the Brunauer Emmett Teller (BET) method and the results are shown in Fig.6. The BET analysis developed in 1938 is the standard method for determining surface areas from N_2 molecules adsorption on the surface.[27] The BET theory can be described as $1/\{v[(P_0/P) - 1]\} = \{c-1\}/\{v_m c\}(P/P_0) + 1/\{v_m c\}$, where P and P_0 are the equilibrium and the saturation pressure of adsorbates, v is the adsorbed gas quantity, and v_m is the monolayer adsorbed gas quantity, c is the BET constant. As shown in Fig.6, $1/\{v[(P_0/P) - 1]\}$ versus (P/P_0) plots exhibit a linear behavior for both the nanorods synthesised at 200 °C and 160 °C. The slope is corresponding to $(c-1)/\{v_m c\}$ and the intercept is $1/\{v_m c\}$. It can be deduced that the specific surface areas are 76.95 m^2/g and 44.52 m^2/g for the nanorods synthesised at 200 °C and 160 °C, respectively, which support our analysis above.

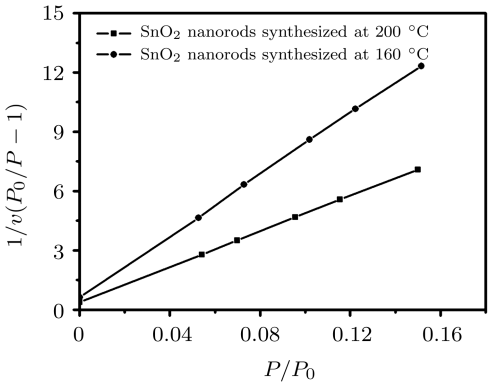


Fig.6. The plots of $1/\{v[(P_0/P) - 1]\}$ versus (P/P_0) show good linearity. The specific surface areas are calculated to be 76.95 m^2/g and 44.52 m^2/g for the nanorods synthesised at 200 °C and 160 °C respectively.

4. Conclusions

In summary, the electrochemical properties of SnO_2 nanorods as anode materials for lithium-ion battery were investigated. The observed initial discharge capacities were much higher than the theoretical values of the bulk SnO_2. The extra Li-storage capacity is mainly corresponding to the interfacial charge storage. During the following 15 cycles, the reversible capacity decreases from 929 to 576 mA·h/g with a fading rate of 3.5% per cycle. The obvious cyclic fading is linked with the volume expansion and SEI films decomposition during cycling. At the end, the size effect of the SnO_2 nanorods on the electrochemical properties is briefly discussed. The nanorods with smaller size were synthesised at 160 °C. They showed much lower reversible capacities than those synthesised at 200 °C, which is mainly due to the smaller specific surface area caused by serious aggregation.

References

[1] Arico A S, Bruce P G, Scrosati B, Tarascon J M and Van Schalkwijk W 2005 *Nat. Mater.* **4** 366

[2] Maier J 2005 *Nat. Mater.* **4** 805

[3] Ohzuku T, Iwakoshi Y and Sawai R 1993 *J. Electrochem. Soc.* **140** 2490

[4] Hou X H, Hu S J, Li W S, Ru Q, Yu H W and Huang Z W 2008 *Chin. Phys.* B **17** 3422

[5] Poizot P, Laruelle S, Grugeon S, Dupont L and Tarascon J M 2000 *Nature* **407** 496

[6] Li W Y, Xu L N and Chen J 2005 *Adv. Funct. Mater.* **15** 851

[7] Li G C, Pang S P, Jiang L, Guo Z Y and Zhang Z K 2006 *J. Phys. Chem.* B **110** 9383

[8] Subramanian V, Burke W W, Zhu H W and Wei B Q 2008 *J. Phys. Chem.* C **112** 4550

[9] Nam K T, Kim D W, Yoo P J, Chiang C Y, Meethong N, Hammond P T, Chiang Y M and Belcher A M 2006 *Science* **312** 885

[10] Hu Y S, Kienle L, Guo Y G and Maier J 2006 *Adv. Mater.* **18** 1421

[11] Courtney I A and Dohn J R 1997 *J. Electrochem. Soc.* **144** 2045

[12] Ahn H J, Choi H C, Park K W, Kim S B and Sung Y E 2004 *J. Phys. Chem.* B **108** 9815

[13] Park M S, Wang G X, Kang Y M, Wexler D, Dou S X and Liu H K 2007 *Angew. Chem. Int. Ed.* **46** 750

[14] Lou X W, Wang Y, Yuan C L, Lee J Y and Archer L A 2006 *Adv. Mater.* **18** 2325

[15] Han S, Jang B, Kim T, Oh S M and Hyeon T 2005 *Adv. Funct. Mater.* **15** 1845

[16] Chen Y J, Xue X Y, Wang Y G and Wang T H 2005 *Appl. Phys. Lett.* **87** 233503

[17] Wen S J and Chen L Q 1996 *Chin. Phys.* **5** 692

[18] Retoux R, Brousse T and Schleich D M 1999 *J. Electrochem. Soc.* **146** 2472

[19] Zhukovskii Y F, Balaya P, Kotomin E A and Maier J 2006 *Phys. Rev. Lett.* **96** 058302

[20] Zhukovskii Y F, Kotomin E A, Balaya P and Maier J 2008 *Solid State Science* **10** 491

[21] Hu J, Li H, Huang X J and Chen L Q 2006 *Solid State Ionics* **177** 2791

[22] Idota Y, Kubota T, Matsufuji A, Maekawa Y and Miyasaka T 1997 *Science* **276** 1395

[23] Vetter J, Novak P, Wagner M R, Veit C, Moller K C, Besenhard J O, Winter M, Wohlfahrt-Mehrens M, Vogler C and Hammouche A 2005 *J. Power Sources* **147** 269

[24] Brousse T, Retoux R, Herterich U and Schleich D M 1998 *J. Electrochem. Soc.* **145** 1

[25] Brousse T, Defives D, Pasquereau L, Lee S M, Herterich U and Schleich D M 1997 *Ionics* **3** 332

[26] Wang J, Polleux J, Lim J and Dunn B 2007 *J. Phys. Chem.* C **111** 14925

[27] Brunauer S, Emmett P H and Teller E 1938 *J. Am. Chem. Soc.* **60** 309